



Modifying the antibacterial performance of Cu surfaces by topographic patterning in the micro- and nanometer scale

Daniel Wyn Müller^{a,b,*}, Christoph Pauly^a, Kristina Brix^c, Ralf Kautenburger^c, Frank Mücklich^a

^a Chair of Functional Materials, Department of Materials Science, Saarland University, 66123 Saarbrücken, Germany

^b SurFunction GmbH, 66123 Saarbrücken, Germany

^c Department of Inorganic Solid-State Chemistry, Elemental Analysis, Saarland University, 66123 Saarbrücken, Germany

ARTICLE INFO

Keywords:

Active antimicrobial surfaces
Biomimetic surface structures
Ultrashort laser pulses
Direct laser interference patterning

ABSTRACT

Antimicrobial surfaces are a promising approach to reduce the spread of pathogenic microorganisms in various critical environments. To achieve high antimicrobial functionality, it is essential to consider the material-specific bactericidal mode of action in conjunction with bacterial surface interactions. This study investigates the effect of altered contact conditions on the antimicrobial efficiency of Cu surfaces against *Escherichia coli* and *Staphylococcus aureus*. The fabrication of line-like periodic surface patterns in the scale range of single bacterial cells was achieved utilizing ultrashort pulsed direct laser interference patterning. These patterns create both favorable and unfavorable topographies for bacterial adhesion. The variation in bacteria/surface interaction is monitored in terms of strain-specific bactericidal efficiency and the role of corrosive forces driving quantitative Cu ion release. The investigation revealed that bacterial deactivation on Cu surfaces can be either enhanced or decreased by intentional topography modifications, independent of Cu ion emission, with strain-specific deviations in effective pattern scales observed. The results of this study indicate the potential of targeted topographic surface functionalization to optimize antimicrobial surface designs, enabling strain-specific decontamination strategies.

1. Introduction

Diseases related to bacterial infections are considered as one of the major future threats for public health, which caused one out of eight deaths worldwide in 2019 [1]. In the same year, biofilm induced economic damage was estimated at more than 4000bn USD, where approx. 30 % are directly related to biofilm burden in the healthcare sector and food production [2]. In close relation, a considerable and ongoing hazard by the increase of bacterial resistance against antibiotic agents is reported. This also affects remote habitats such as the international space station (ISS) [3,4]. In case of bacterial spread in public and remote environments, contact surfaces represent one of the dominant distribution routes. This has recently been demonstrated by microbial tracking on the ISS, where the overall space station microbiome was shown to be dominated by bacterial strains associated with the human skin [5]. Multiple strategies to reduce the formation of biofilms and the viability of pathogenic microorganisms on technical as well as frequently contacted surfaces have therefore been investigated in the recent two decades. A variety of acting mechanisms can be utilized, here, without the need to involve antibiotic agents.

The two most investigated and applied strategies are active antimicrobial substrate materials like silver (Ag) and copper (Cu) and bactericidal or contact guiding surface topographies [6–9]. The antimicrobial activity of Ag- and Cu based substrates is directly linked to the quantity of electrochemically emitted ions, which are toxic to most microorganisms [10,11]. Here, Cu proves to be particularly interesting due to extended environmental applicability [12], its higher broadband effect [11], lower human toxicity threshold [13,14] as well as economically more favorable and broad availability in technically applicable alloy systems. Cu mediated bacterial deactivation is related to several modes of action including membrane damage, formation of reactive oxygen species (ROS) via Fenton-type reaction and structural damage against DNA as well as protein molecules due to its high thiophilicity [15,16]. Certain guidelines need to be followed to achieve high antimicrobial efficiency of Cu surfaces. This includes a close contact between bacteria and Cu emitting agent [17], as well as the avoidance of chemical surface contamination [18].

Biomimetic surface patterns on inert substrates utilize self-cleaning and bactericidal surface properties based on the functionality of μm - and nm -scaled topographies found, e.g., on *lotus* leaves [19] or *cidada*

* Corresponding author at: Chair of Functional Materials, Saarland University, Post Office Box 151150, 66041 Saarbrücken, Germany.

E-mail address: daniel.mueller@uni-saarland.de (D.W. Müller).

<https://doi.org/10.1016/j.bioadv.2025.214184>

Received 5 September 2024; Received in revised form 7 January 2025; Accepted 9 January 2025

Available online 10 January 2025

2772-9508/© 2025 The Authors. Published by Elsevier B.V. This is an open access article under the CC BY license (<http://creativecommons.org/licenses/by/4.0/>).

and dragonfly wings. How bacterial surface interaction is modulated on these surfaces relates to the topographic pattern scale. Pillar like patterns at a scale below 200 nm following the design of cicada or dragonfly wings have been shown to exhibit bactericidal properties where adherent bacterial cells are deactivated by mechanical membrane rupture [8,20]. On surface patterns with topographic feature sizes in the upper sub- μm range, bacterial interaction was found to switch from bactericidal to contact inhibition [21,22]. Further enlargement of the pattern scales up to the size of a single bacterial cell and beyond ultimately leads to improved bacterial adhesion and retention [9,23,24]. Here, contact guidance impacting cell orientation and initiation of bio-film formation can be achieved by targeted surface design [9,25]. How the actual scale of topographic surface patterns affects bacterial response may vary significantly between different bacterial strains [21,26], indicating a very complex interaction between the bacterium and the patterned surface. In fact, secondary surface properties were shown to play an important role in antimicrobial surface functionality, since mechanically induced killing or the attachment/repulsion of individual bacteria is driven by attraction and bonding forces. These forces depend, e.g., on environmental conditions [27], surface charge [28] and wettability [29,30].

More recently, antimicrobial surface design aims to agitate or combine the previously mentioned modes of action [31,32] which has already been shown to potentially improve inherent bactericidal surface properties. Functional coatings on topographically patterned inert surfaces have been proven to reduce bacterial viability either by inducing a positive surface charge that affects membrane integrity [33], or by adding the active killing capacities of Ag and Cu [34]. The application of Cu has also been investigated as nanoparticles (NP) in surface decoration or as a complementing composite in coatings, where the NP shape aims to facilitate aggregation on bacterial membranes up to intrusion [35,36]. More recently, it has been found that the antibacterial effect of Cu NP is closely linked to the quantitative release of Cu ions, while an actual intrusion into bacterial cells does not occur [37]. Recent functionalization to enhance the antimicrobial efficacy of Cu surfaces involves the combination with mechanically induced antimicrobial properties of cicada and dragonfly wing, such as nm-scale surface features piercing bacterial cell walls [38,39]. Depending on the methodology used, Cu ion release might however be negatively affected by excessive oxide formation, here [40,41]. In another approach, the surface/area ratio of bulk Cu is exponentially increased by inducing a super-hydrophilic mesh-like porous morphology, which in parallel enhances the initial Cu ion release and bactericidal activity [42]. In another study, topographic surface patterns at the scale of a single bacterium were shown to enhance antimicrobial efficacy with lesser dependence on quantitative Cu ion release [43]. Here, the decrease of bacterial viability was discussed to be related to functional properties of the substrate surface, including both topography and wettability, which affect bacteria/surface bonding and, in parallel, the bacterial sensitivity against Cu.

The current state of research on bactericidal surfaces highlights the complexity of the underlying mechanisms being involved in the actual expression of antimicrobial effects within the different surface design strategies. To achieve a sustained high decontamination efficiency, the actual bacteria/surface interaction must be actively tailored to agitate the focused mode of action by surface design. In this context, the aim of the presented study is to investigate how bacterial contact modulation by topographical surface design impacts the antibacterial efficacy of Cu surfaces. Line-like periodic surface patterns are generated using ultra-short pulsed direct laser interference patterning (USP-DLIP), which topographically modulate the contact surface available for the adhesion of individual bacterial cells. The resulting impact on the antimicrobial efficacy of Cu surfaces against rod-shaped gram-negative *Escherichia coli* K12 (BW25113) and spherical gram-positive *Staphylococcus aureus* SA113 is investigated in a complementary approach applying water contact angle measurement (CA) confocal laser scanning microscopy

(LSM), high resolution electron beam analysis (FIB/SEM/EDS), grazing incidence X-ray diffractometry (GI-XRD) and wet plating. Improved comprehension of the influence of modified bacterial contact conditions on bactericidal efficacy of actively antimicrobial substrate surfaces potentially allows for a better conception of decontamination measures in various partly critical environments [6,7,31].

2. Results and discussion

2.1. Initial surface state

Line-like surface structures exhibiting pattern periodicities of 3 μm ($P > Bac$), 1 μm ($P \approx Bac$) and 750 nm ($P < Bac$) are generated on pure Cu surfaces via USP-DLIP with respect to the single cell dimensions of the two bacterial strains involved in this study (see Fig. 1). The actual bacterial contact conditions on these surfaces result from the individual surface geometries including concave (valley areas) and convex (peak areas) sections. The primary pattern geometry with a periodicity of 3 μm exhibits a valley width of $2.08 \pm 0.14 \mu\text{m}$ and depth of $1.1 \pm 0.15 \mu\text{m}$, which enables complete intrusion of single cells and clusters. On 1 μm patterns, the valley width of $0.81 \pm 0.07 \mu\text{m}$ approximates the single cell dimensions of both parallelly aligned *E. coli* and *S. aureus*, which facilitates single cell contact combined with the low pattern depth. The valley width of approx. 0.54 μm on 750 nm patterns finally ranges below the single bacterial cell diameter, by which the valley floor is not fully accessible for adherent bacteria at the present pattern depth. In parallel to the described primary pattern geometry, the surface design involved tailoring of the sub-pattern formation by material specific thermodynamic response according to the aspired contact conditions [44].

In parallel to topographic surface modification, an agglomeration of nm-scaled oxidic redepositions during USP-DLIP processing was previously described on Cu [45]. The redeposited oxide particles have been shown to mainly consist of Cu_2O and scale with the amount of ablated matter as well as the fluence applied [44]. Accordingly, the Cu_2O (111) signal measured by grazing incidence X-ray diffraction (GI-XRD) indicates a more pronounced agglomeration of process-induced surface oxides on as-processed 3 μm patterns in comparison to 1 μm and 750 nm (see Fig. 2a) corresponding to the respective ablated volume. Post-processing by immersion etching in citric acid induces a reduction of the oxide signal as visible in Fig. 2a, which can be attributed to the removal of oxidic process agglomerates [45]. The stable but low CuO signal intensity fits to the previously suggested oxidation mechanism, where this oxide phase is mainly formed as a superficial layer during consecutive atmospheric passivation [45].

In bacterial adhesion to technical surfaces, physicochemical surface properties were shown to play a parallel role to surface topography and might furthermore impact bactericidal efficacy [29,43,46]. This includes e.g. surface wettability corresponding to acid-base interactions [47]. Wettability of laser processed metallic surfaces is impacted by atmospheric aging as well as hierarchical pattern morphologies [48], which is confirmed by comparison of the contact angles (CA) measured on as-processed and immersion etched USP-DLIP Cu surfaces after three weeks of aging (displayed in Fig. 2b). Wettability is consistently reduced on the USP-DLIP surfaces, while the hydrophobic wetting behavior is enhancing alongside increasing pattern scale. In between similar pattern periodicities, the as-processed surfaces exhibit elevated hydrophobic surface properties over the immersion etched topographic counterparts suggesting an additional contribution of the nm-scaled oxide particles.

Both, the high CA values, as well as the roll-off/sticking behavior on the 3 μm samples are consistent with previous results indicating a Cassie-Baxter wetting state on as-processed and Wenzel wetting on immersion etched surfaces [43]. A pronounced difference between CA on as-processed and immersion etched samples can be observed for less hydrophobic 1 μm and 750 nm patterns. CA anisotropy on the isotropic surface patterns remains close to 1.0 along reducing CA for 3 μm and 1 μm indicating a low pinning effect on droplet propagation. Surface

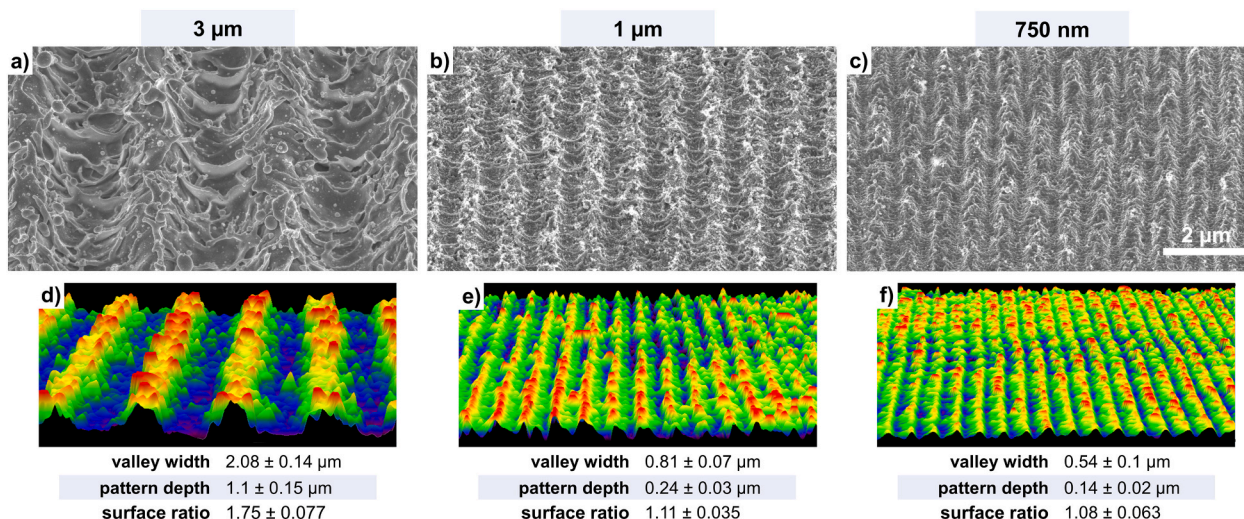


Fig. 1. SEM images of line-like periodic surface patterns in the scale of 3 μm ($P > Bac$), 1 μm ($P \approx Bac$) and 750 nm ($P < Bac$) applied on the Cu surfaces: a-c) SEM imaging, where the 3 μm pattern was previously immersion etched, while 1 μm and 750 nm represent the as-processed state. d-f) representative topographic profiles of 3 μm, 1 μm and 750 nm patterns detected via CLSM also listing the deviation of corresponding pattern geometry parameters relevant for bacterial contact investigation between the different substrates.

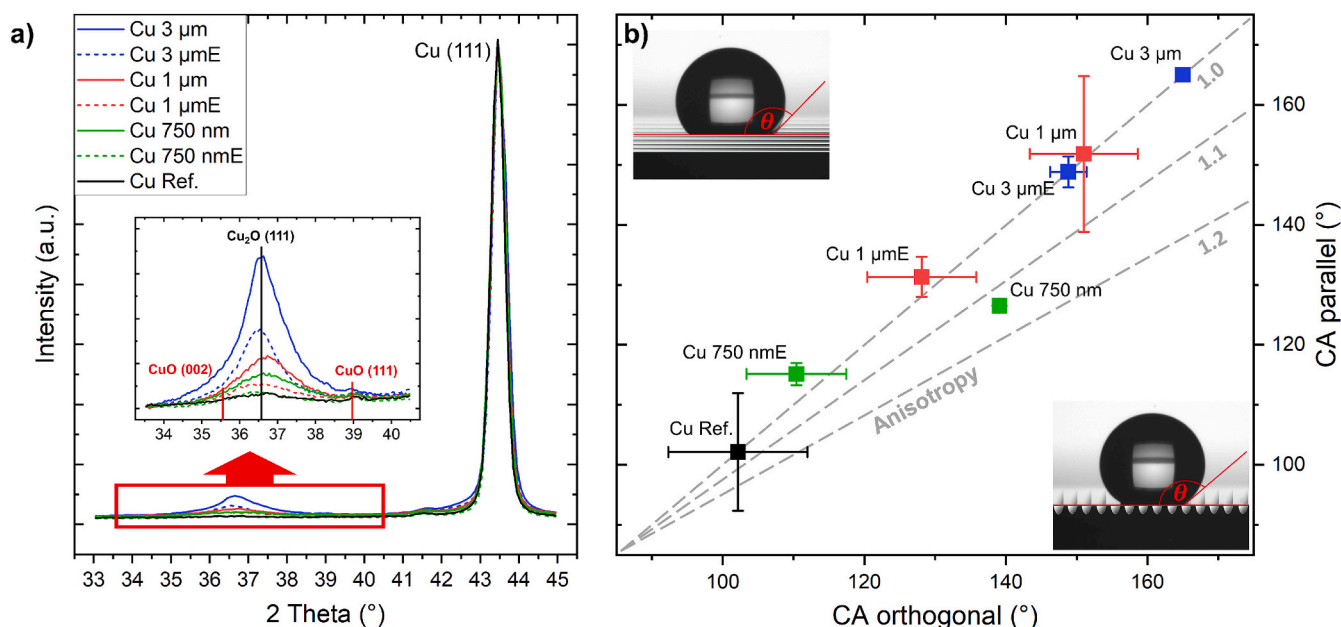


Fig. 2. Process related modification of surface chemistry impacting functional aspects: a) alteration of surface oxidation after USP-DLIP patterning in as-processed and immersion etched state (E). b) stabilized surface wettability of the polished reference (Steel Ref., Cu Ref.) and USP-DLIP patterned Cu and stainless steel surfaces at 3 μm, 1 μm and 750 nm pattern periodicity after three weeks of aging under ambient atmosphere. Cu USP-DLIP surfaces are represented both in as-processed and immersion etched state.

wetting on 750 nm patterns exhibits a deviating behavior, where increased CA anisotropy in the as-processed state indicates pinning along the structure peaks, which is eliminated after immersion etching.

2.2. Antimicrobial properties vs. bacteria/pattern scale ratio

Both gram-negative *E. coli* and gram-positive *S. aureus* have been exposed to as-processed and immersion etched USP-DLIP Cu surfaces by wet plating using mirror-polished samples of both bactericidal Cu and inert steel as topographically smooth reference surfaces. Strain specific exposure times were chosen to allow for the determination of topography related differences in bacterial viability with respect to the individual survival rates. The time-resolved reduction of viable bacterial cell

count for both *E. coli* (blue) and *S. aureus* (green) is illustrated in Figs. 3 and 4, each complemented by the corresponding Cu ion release. The line graphs represent experimentally measured bacterial viability/dissolved Cu while the bar graphs represent the respective time- and area-dependent killing rates normalized by the surface ratio measured in LSM analysis. The factor of in- or decrease in relation to the smooth Cu reference is stated for each data-point of the USP-DLIP patterned surfaces in the bar graphs.

Bacterial cells of both strains were found to be rapidly killed on Cu surfaces with a reduction in viable cell count of >3 log already after 60 min of exposure, affecting the majority of the USP-DLIP surfaces as well as the Cu reference surfaces tested. Extended exposure times of up to 120 min resulted in complete inactivation of bacterial cells on all tested

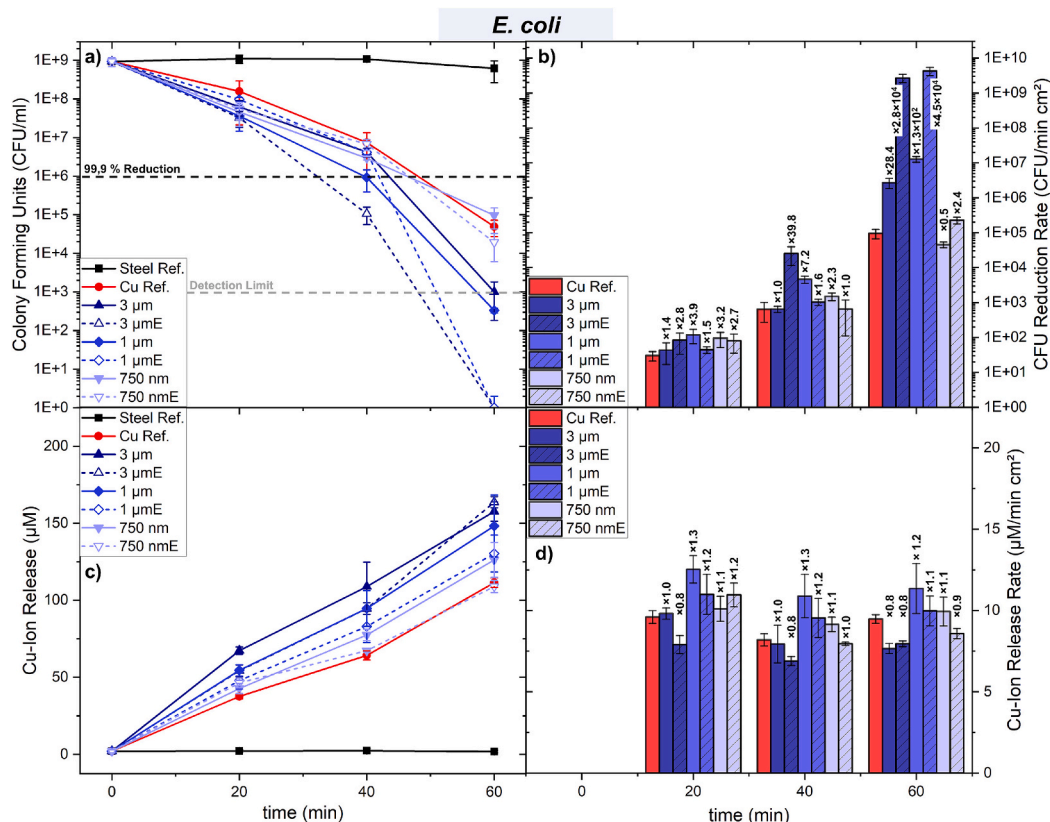


Fig. 3. a, b) Bacterial viability and c, d) respective Cu ion release rates measured via wet plating and inductively coupled plasma triple quadrupole mass spectrometry (ICP-QQQ) for *E. coli*. Exposure times were chosen as 20, 40 and 60 min. Line graphs represent the measured a) colony forming units (CFU) and c) quantitative Cu ion release. The bar graphs show the time dependent development of b) bacterial killing and d) Cu emission rates per area, corrected for the topography related increase in surface ratio complemented by the factor of in- or decrease observed on USP-DLIP surfaces in comparison to the smooth Cu reference surfaces.

surfaces, which was also found in additional test series after 90 min of exposure. Deviations in bacterial viability between the different USP-DLIP patterned Cu surfaces are well displayed after 60 min of exposure, before complete bacterial deactivation is initiated universally. USP-DLIP surface modification is found to exhibit a significant impact on bacterial viability, where both agitation and depletion of the bactericidal capacities of smooth Cu surfaces can be observed on the different pattern scales with varying dependency on the bacterial strain tested.

In case of *E. coli* initial bacterial killing on USP-DLIP patterned surfaces consistently levels above topographically smooth Cu within the first 40 min of exposure (see Fig. 3a). The observed differences between individual USP-DLIP surfaces do not follow a clear dependency on pattern scale or post-processing state, where the highest initial killing rates are distributed between immersion etched 3 μm followed by as-processed 1 μm and 750 nm. This is however altered after 60 min, where the post-processed surface state appears to play an additional dominant role aside of actual primary pattern scales. Here, bacterial inactivation is consistently higher on immersion etched surfaces compared to their as-processed counterparts of similar primary surface pattern. This is particularly evident for 3 μm and 1 μm structures with primary pattern geometries that are geometrically favorable for increased bacterial contact area: No remaining viable bacteria could be determined on etched surfaces, while the viable cell count still ranges close to the experimental detection limit on as-processed samples. In the case of 750 nm pattern scales, bacterial deactivation lies either within or below the range of the smooth Cu reference throughout 60 min of exposure. Independent of the post-processing state, samples of 750 nm pattern periodicity exhibit considerably lower bactericidal activity compared to 3 μm and 1 μm on which the bacterial killing rate ranges three to four orders of magnitude above the smooth reference (displayed

Fig. 3b). On as-processed 3 μm and 1 μm USP-DLIP surfaces, a higher antibacterial efficacy of 1 μm (2 log increase of killing rate) over 3 μm (1 log increase of killing rate) against *E. coli* is observed. Overall, the bactericidal effect of the different surface topographies against *E. coli* scale as 1 μm ($P \approx \text{Bac}$) > 3 μm ($P > \text{Bac}$) >> 750 nm ($P < \text{Bac}$) \approx smooth. The post-processing state appears to have a similarly pronounced impact as the primary DLIP pattern size, scaling with immersion etched > as-processed in antibacterial efficacy.

Initial bacterial killing within the first 30 min of exposure exhibits a pronounced lag phase for *S. aureus*, where CFU reductions remains below the values of smooth Cu on most USP-DLIP surfaces (see Fig. 4a and b). Similar to *E. coli*, differences in topography mediated bactericidal efficacy between the surfaces tested are most evident after 60 min. In case of contact promoting surface topographies, post-processing by immersion etching also leads to higher bacterial deactivation within similar pattern scales, which is however inverted at 750 nm. In contrast to *E. coli*, the primary pattern scale appears to have a higher effect on bactericidal efficacy than the post-processing state. The highest bacterial inactivation rate is observed on 3 μm surface patterns exhibiting bacterial viability close to the detection limit. A 1 log increase of bacterial killing compared to smooth reference surfaces can furthermore be detected on immersion etched 1 μm patterns. Bactericidal efficacy is not promoted by USP-DLIP processing in case of as-processed 750 nm patterns and even reduced on as-processed 1 μm as well as etched 750 nm surface patterns. In summary, the antibacterial efficacy of the tested surface topographies against *S. aureus* scales as 3 μm ($P > \text{Bac}$) >> 1 μm ($P \approx \text{Bac}$) >/< smooth >/= 750 nm ($P < \text{Bac}$). The post-processing state shows a similar relation of immersion etched > as-processed like for *E. coli*, but with a lower overall impact on bactericidal activity.

The Cu ion release parallelly monitored during Cu exposure of *E. coli*

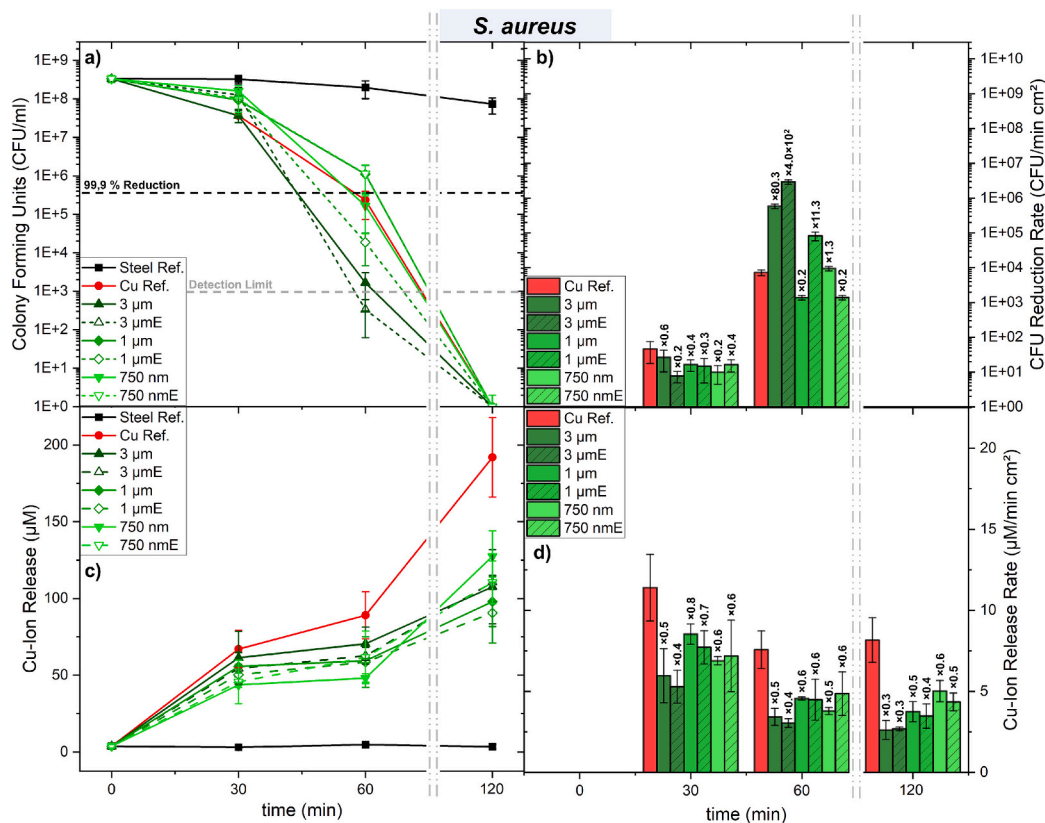


Fig. 4. a, b) Bacterial viability and c, d) respective Cu ion release rates measured via wet plating and inductively coupled plasma triple quadruple mass spectrometry (ICP-QQQ) for *S. aureus*. Exposure times were chosen as 30, 60 and 120 min, displayed with a shortened time axis. Line graphs represent the measured a) colony forming units (CFU) and c) quantitative Cu ion release. The bar graphs show the time dependent development of b) bacterial killing and d) Cu emission rates per area, corrected for the topography related increase in surface ratio complemented by the factor of in- or decrease observed on USP-DLIP surfaces in comparison to the smooth Cu reference surfaces.

exhibits a clear relation to surface area enhancement by USP-DLIP where the Cu emission rate appears to level with increasing pattern scale (displayed in Fig. 3c). The surface ratio equalization of Cu ion release in Fig. 3d shows an almost similar release rate of Cu ions between the different Cu surfaces, with only 3 μm textured surfaces showing lower values compared to the Cu references. Between similar pattern sizes Cu ion release tends to be higher on as-processed surfaces, which appears to be linked to the dissolution of the process-induced oxide particles as recently shown in a preliminary study [49]. In contrast, the relation of Cu ion release between USP-DLIP and smooth reference surfaces is inverted in the case of *S. aureus*, where the reference surfaces exhibit the highest Cu emission (compare Figs. 3c, d and 4c, d). Nevertheless, bacterial killing rates of *S. aureus* on 3 μm and immersion etched 1 μm patterns are one to two orders of magnitude higher than the reference surfaces. In fact, bacterial viability is found to not necessarily correlate to the amount of Cu emission for both tested strains. E.g., Cu ion release on immersion etched 3 μm and 1 μm usually falls below the values of as-processed surfaces, while the corresponding killing rates after 60 min exposure against *E. coli* and *S. aureus* exhibit an inverse relation. Cu release from immersion etched 1 μm surfaces exposed to *E. coli* inoculated bacteria testing solution (BTS) remains at similar magnitudes like as-processed 750 nm, whereas bacterial killing rates of both sample types occupy the opposite ends of the bactericidal efficiency spectrum after 60 min of exposure. Likewise, the bactericidal efficiency of the smooth Cu reference surfaces against *E. coli* surpasses that of the as-processed 750 nm patterns, although the respective Cu ion release is lower.

In parallel to the lower Cu emission on USP-DLIP surfaces exposed to *S. aureus*, the total amount of dissolved Cu appears to stagnate between 30 and 60 min of exposure, while bacterial viability undergoes a

significant decline within this period. After 120 min of exposure, a further increase in the dissolved Cu content can be observed in Fig. 4c, coupled with complete bacterial inactivation of *S. aureus*. Here, the release of Cu ions on the 750 nm patterns shows an altered trend, eventually surpassing the values of the other USP-DLIP patterns despite a lower surface ratio. These combined observations indicate both, a different bacteria/surface interaction between the tested bacterial strains and a modulation of antibacterial efficacy by USP-DLIP, which is not necessarily linked to Cu ion release rates. Aside of a potentially beneficial effect of hydrophobic surface wetting [43], differences in CA between the tested surface types do not appear to allow a direct correlation to bactericidal activity.

In view of the topography specific deviation in antibacterial efficacy, a closer look is taken on the individual contact conditions established alongside Cu exposure by post-mortem SEM analysis of bacterial allocation on the different topographies.

2.3. Impact of topographic contact conditions on bacteria/surface interaction

To gain insight into the actual bacterial contact conditions involved in the expression of Cu sensitivity on the different surface topographies, SEM analysis of the bacterial interaction with the Cu surfaces was conducted after either 60 min (*E. coli*) or 90 min (*S. aureus*) of exposure. A capability of cell-cluster agglomeration can be determined on 3 μm patterned surfaces ($P > Bac$) for both *E. coli* (blue) and *S. aureus* (green) due to the increased valley dimensions, as visible in Fig. 5a and b. On both 1 μm ($P \approx Bac$) and 750 nm ($P < Bac$), surface attachment was found to be more likely to occur in the single cell domain in case of *E. coli*, while *S. aureus* remains clustered. Single cells of *E. coli* are

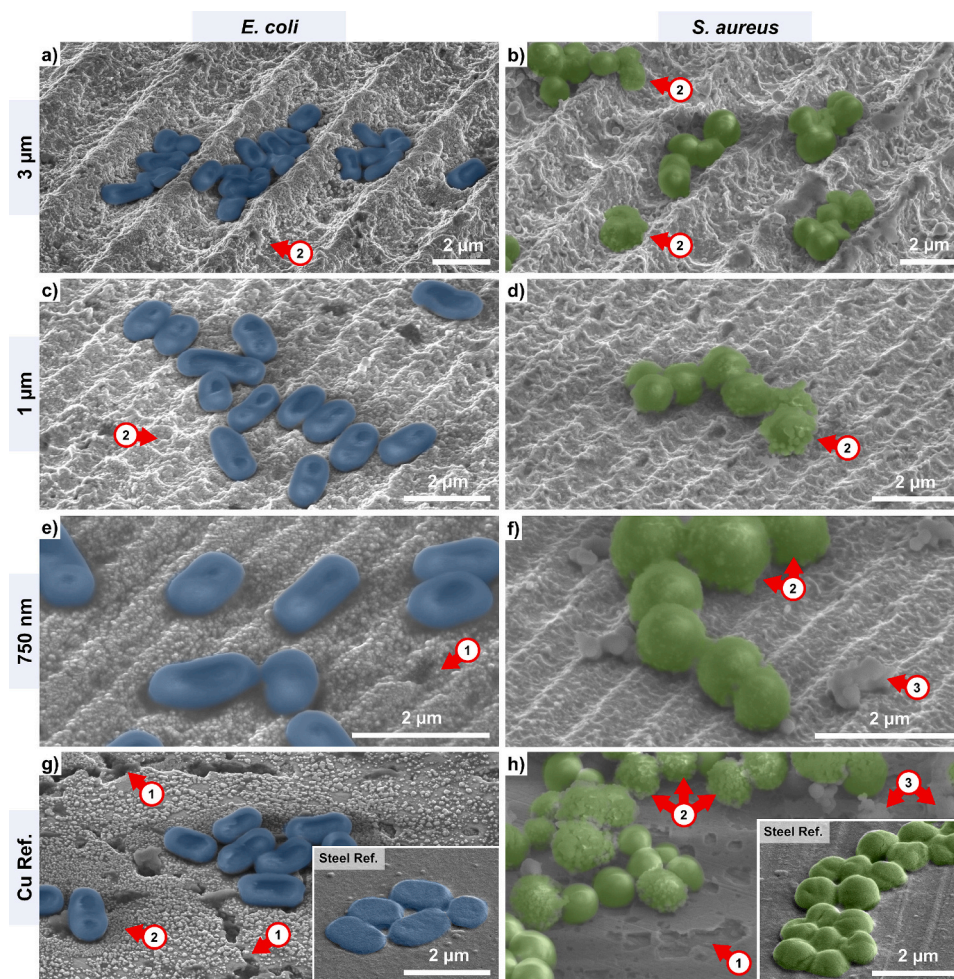


Fig. 5. Representative images of the SEM analysis on topography related contact conditions for single bacterial cells and cell-clusters on immersion etched USP-DLIP and polished Cu reference surfaces. Single cells of *E. coli* (blue) and *S. aureus* (green) are shown in exposure to a, b) 3 μm ($P > \text{Bac}$), c, d) 1 μm ($P \approx \text{Bac}$) and e, f) 750 nm ($P < \text{Bac}$) pattern scale as well as g, h) Cu Ref. surfaces exhibiting varying impact on cell-adhesion. The bacterial cell morphology observed on inert stainless steel references is provided by an inset in both g) and h) for each strain. Several modifications on the substrate surfaces arising from chemical interaction during BTS exposure are highlighted in the images corresponding to (1) corrosive surface deterioration, (2) redepositions in the vicinity (*E. coli*) or attached (*S. aureus*) to bacterial cells, (3) weakly attached globular particle clusters. Imaging was done utilizing SE contrast on uncoated samples under 52° tilt. (For interpretation of the references to colour in this figure legend, the reader is referred to the web version of this article.)

frequently aligned in parallel orientation to the line-like surface pattern on 1 μm (Fig. 5c), while they are more randomly oriented and less elongated on 750 nm (Fig. 5e), which might indicate unfavorable bacteria/surface contact conditions for these pattern scales, similar to previous findings [23]. Individual *S. aureus* cells appear to be torn between increasing their surface contact area and maintaining connections with neighboring cells on both 1 μm and 750 nm surface patterns, where individual cells also adhere to pattern peaks due to spatial restrictions within the small interconnected cell clusters (Fig. 5d and f). The cell-cluster size on the mirror-polished reference surfaces is similar to 3 μm for *E. coli*, while it is increased for *S. aureus* compared to the topographic surface patterns, highlighting the strain's preference for cell-cell connectivity. In fact, cell-wall associated macromolecules involved in surface adhesion of *S. aureus* have been reported to be similarly related to cell-cell connectivity and biofilm formation [50], where intercellular connectivity might be considered to be of similar importance as quantitative surface contact for single cell viability. Depending on the combination of topographical and chemical surface properties present, intercellular bond strength may outweigh the bacteria/surface bond strength [29,51].

Surface contact conditions have been shown to influence bacterial response mechanisms involving, e.g., the triggering of biofilm formation

and stimulated metabolic activity [28]. In parallel, quantitative Cu uptake by viable bacteria has previously been discussed as being facilitated by respiratory activity, which leads to an accelerated cell-damaging rate [16]. In fact, bacterial killing was found to be significantly enhanced on surface patterns where an increased bacterial contact was observed for both strains independent from quantitative Cu ion release. In view of the bactericidal activity measured, cavity dimensions that allow for cell-cluster adhesion on 3 μm patterns seems to be effective to increase antimicrobial efficiency against both *E. coli* and *S. aureus*. An elevated Cu sensitivity on 1 μm patterns was in turn solely found for *E. coli*, which predominantly showed single cell adhesion that allows for increased single cell contact on this surface type. A low up to inverted impact on bactericidal effectivity can finally be observed on the 750 nm pattern scale for both strains. In previous studies, reduced biofilm growth after extended exposure times could be ascertained for *E. coli* on comparable sub- μm topographies, which was however not the case for *S. aureus* that rather exhibited a higher adaptivity [21,26]. A recent publication linked surface adhesion of *S. aureus* to functional membrane sites, which are heterogeneously distributed across the cell envelope and display a characteristic patchiness that appears to befit this pattern periodicity [52]. This might improve surface adhesion of *S. aureus* on line-like 750 nm patterns in an extended time frame, whereas initial bacterial

adhesion related to the rapid onset of the antibacterial mechanism of Cu surfaces might still be restrained within the time scales of the wet plating experiments.

2.4. Bactericidal interaction with the Cu substrate

The notable deviation of Cu ion emission between *E. coli* and *S. aureus* with inverse relation of USP-DLIP patterned to smooth surfaces indicates a different chemical surface interaction of the two bacterial strains (compare Figs. 3c and 4c). Quantitative ion release on Cu surfaces exposed to bacteria inoculated PBS has previously been shown to be majorly dependent on the corrosive interaction between the Cl⁻-containing medium and substrate, where bacteria might act as corrosion catalysts due to the impairment of surface passivation by Cu ion scavenging [53]. This mechanism has been shown to be enhanced in case of lysed bacterial cells [40,53] indicating a protective role of intact cell membranes. In the absence of bacterial cells, USP-DLIP Cu surfaces form a stabilized oxide layer preventing further surface degradation and Cu dissolution within 1 h of exposure to PBS indicated by a reduced Cu ion release rate [43].

In this study, the Cu ion release from USP-DLIP patterned Cu surfaces exposed to *E. coli* inoculated PBS exhibits a constant Cu release above the level of mirror-polished Cu, befitting the previously described catalytic behavior [53]. Under exposure to *S. aureus* inoculated PBS, Cu ion emission exhibits a closer correlation to stabilizing passivation without a bacterial impact on corrosion behavior presenting a similar relation between USP-DLIP patterns and the smooth reference surfaces [43]. This observation might be related to different cellular response mechanisms involved in the higher Cu resistance reported for gram-positive bacteria [6]. This may also be linked to the stagnation of Cu ion release between 30 and 60 min, as well as the lower bacterial inactivation rates of *S. aureus* within the first 60 min of exposure.

Comparing the corrosive degradation of Cu surfaces alongside BTS exposure, pitting corrosion sites related to grain boundaries or intragranular corrosion are evident on mirror-polished surfaces, while localized corrosion is less evident on USP-DLIP treated surfaces (indicated by (1) arrows in Fig. 5). This corresponds to previous investigation of corrosion kinetics of USP-DLIP processed Cu surfaces [49]. In the case of *E. coli*, corrosion products appear to agglomerate preferentially in the form of a condensing layer of Cu oxide particles close to cell clusters, surrounded by an outer ring of corrosion sites ((2) arrows in Fig. 5a, c and g). The pH value of *E. coli* inoculated PBS has been shown to undergo an alkaline shift favorable for Cu₂O formation [53] alongside Cu surface exposure, whereas preferential agglomeration sites in vicinity to *E. coli* clusters are potentially related to electrochemical microcell formation and mass transport under involvement of the bacterial cells [54]. Regarding *S. aureus*, USP-DLIP patterned Cu surfaces exposed to BTS exhibit considerably less degradation of the substrate surface and thicker oxide layers, indicating better surface passivation when combined with the comparably low Cu ion release rates measured [49]. Instead, particulate adsorbates on bacterial cells can be observed ((2) arrows in Fig. 5b, d, f and h) which vary in quantity and size. Further agglomerations of circular particles can be found with loose connection to the substrate surface ((3) arrows in Fig. 5f and h), which are more likely to be suppressed under *E. coli* BTS exposure.

Comparative consideration of both the difference in corrosive surface deterioration and Cu ion release between *E. coli* and *S. aureus* suggests a deviation in the chemical bacteria/surface interaction for the gram-positive strain from the previously described involuntary Cu drainage of *E. coli* [40,53]. Corrosion catalysis by Cu scavenging of *E. coli* was similarly determined on USP-DLIP Cu surfaces in saline environment in a recent study, where USP-DLIP was also found to increase the corrosion resistance of Cu surfaces by severe mechanical defect implantation [49].

To gain a better understanding of the underlying mechanisms in bacteria/surface interaction occurring alongside deactivation of

S. aureus, alteration of bacterial cell morphology has been investigated in SEM analysis after 90 min of exposure to the Cu surfaces. Prior to SEM analysis a nm-thick sputter-coating of Au₈₀Pd₂₀ was applied on one sample batch to enable high resolution (HR) analyzation and to provide a contrasting layer to distinguish the original sample surface from the deposited Pt-cover layer in FIB cross-sections. HR imaging of *S. aureus* cells exhibits a considerable agglomeration of particles on and partially around bacterial cells (displayed in Fig. 6a and e). These can be separated by morphology and local concentration into two groups, where small spherical particles (SP, blue arrows) tend to fully cover single bacterial cells, while larger particles (LP, red arrows) vary in shape and size without local reference to each other. FIB cross-sectioning reveals varying surface contact angles of SP to the bacterial cell as well as a bright SEM contrast that points towards heavy, non-organic element composition (illustrated in Fig. 6b and highlighted in Fig. 6c). LP in turn constantly exhibit low contact angles to the bacterial surface and a dark SEM contrast similar to the bacterial cell (Fig. 6d). However, in case of further enhanced particle sizes, also the previously dark contrasted LP begin to display an increasing contrast brightening in FIB cross-sectioning indicating the agglomeration of heavier elements (see Fig. 6e and f). LP show a weak structural stability against electron beam irradiation (visible in the cross-section of the particle in Fig. 6g), indicating a partly organic composition.

EDS analysis under low acceleration voltage reveals that both types of particles contain considerable amounts of Cu combined with trace elements C, N and Na originating from the bacterial matrix. An increased Cu content is additionally indicated by a bright Z-contrast in backscatter electron (BSE) imaging that deviates from the bacterial cell envelopes, as displayed in Fig. 7a and c. Both particle types appear in different sizes, suggesting a continuous particle growth after nucleation onto the bacterial cell membranes. Aside of morphology, the two identified particle types differ in composition, where SP exhibit increased intensities of both O and P (see Fig. 7a). This composition implies the formation of cupric phosphate (Cu₃(PO₄)₂) on the bacterial membrane, whereas the unconnected spherical particle clusters at the periphery of the bacterial cells can also be assigned to this particle group according to their EDS spectrum (compare Fig. 7b) [55]. Cu phosphate has previously been identified as a corrosion product formed on Cu surfaces under PBS exposure [55], whereas its formation might be decreased in the presence of *E. coli* due to the reduced availability of free Cu ions in solution and allocated to destroyed bacterial cells [53]. Phosphate formation has been shown to be triggered in the vicinity of bacteria under certain conditions, where the membrane acts as a nucleation site through the catalytic effect of specific membrane molecules and metabolites [56], which may cause the spatial correlation between bacteria and phosphate formation observed here. Further particle growth on *S. aureus* cells indicates a predominant activity of the Cu phosphate formation driving force with an involuntary role of the subjected bacteria, where phosphate formation has been shown to potentially involve chemical dissolution of bacterial biomass [57].

In contrast, LP exhibit increased Cu levels combined with traces of Cl, whereas P is completely absent. Considering the shape and imaging contrast at early formation stages and after further growth, Cu particle formation on *S. aureus* might be linked to defects in the bacterial cell membrane, where exposed cytoplasm triggers a localized agglomeration of Cu (further analysis of Cu particle formation is provided as Supporting Information). Both bacterial Cu scavenging and phosphate formation were found to be enhanced in the case of previously lysed bacteria, where accessible cytoplasm appears to play the major role within the underlying chemical processes of bacterial Cu uptake with membrane integrity as the limiting factor [40,53,56,57]. Nucleation and growth of Cu based agglomerates has previously been found to disrupt bacterial cell wall integrity due to the opposing charging between Cu ions and the membrane that leads to a reduction in membrane Zeta-potential. The resulting avalanching cell wall collapse exposes the bacterial cytoplasm and allows for elevated intracellular Cu ingress [36,58]. Accordingly,

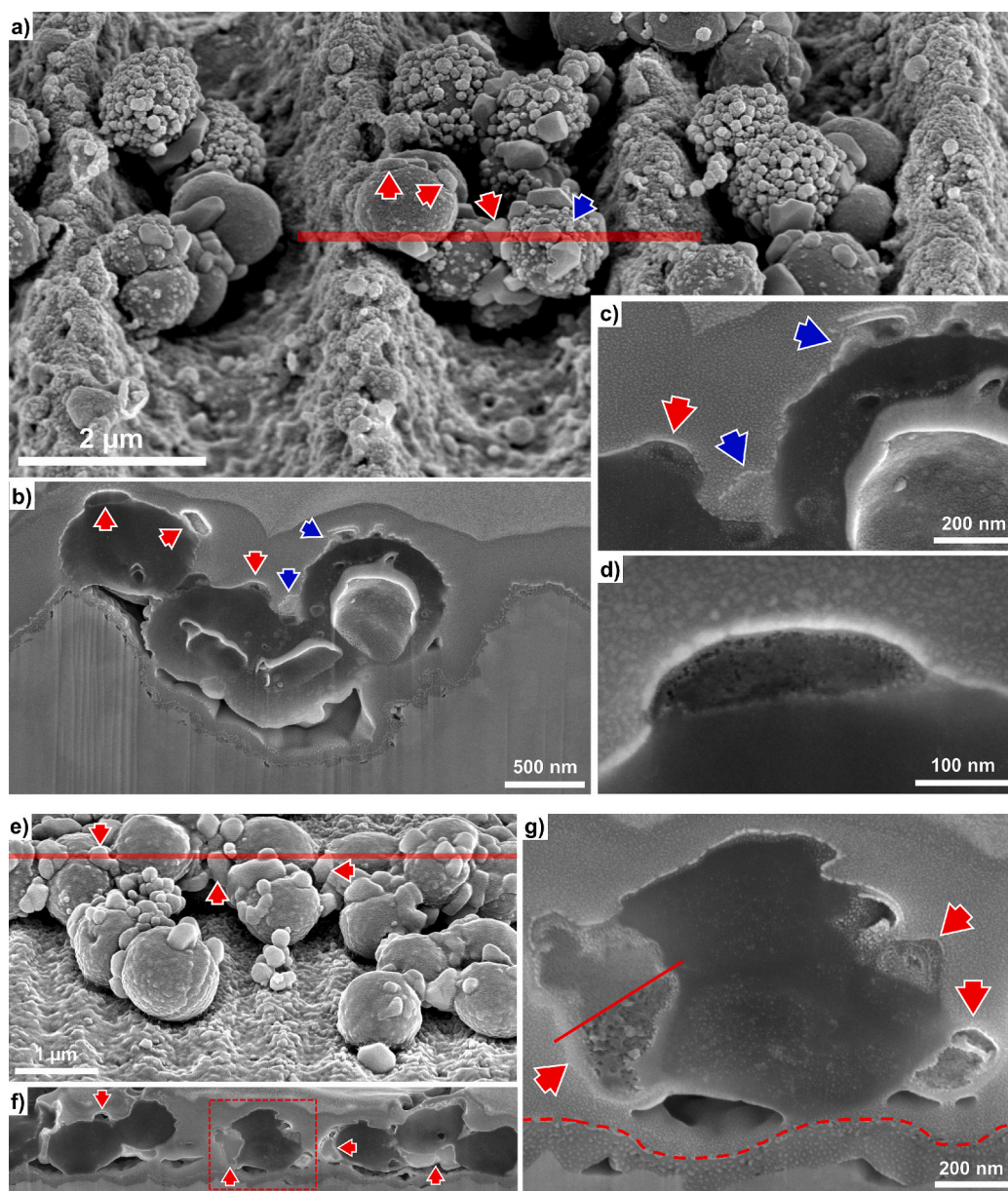


Fig. 6. SEM-imaging of *S. aureus* cells after 90 min of exposure on Cu surfaces. a) Cell-clusters on a 3 μm pattern exhibiting different types of particle agglomerations marked with red (large single particles) and blue arrows (small spherical particle accumulations). The red line indicates the location of the FIB cross-section displayed in b-d). e) Cell-cluster on a 750 nm pattern mainly exhibiting large particle agglomerations, which appear to affect bacterial integrity further highlighted via FIB cross-sectioning in f) and g). Particles are not stable under electron beam irradiation as indicated by structural alteration of the left particle in g) after single (upper part) and multiple imaging (lower part). Imaging was conducted in SE-contrast at 52° sample tilt. (For interpretation of the references to colour in this figure legend, the reader is referred to the web version of this article.)

S. aureus bacterial cells that show increased agglomeration of LP present both a brightened Z-contrast and higher levels of intracellular Cu monitored by EDS in comparison to bacteria lacking LP accumulation (displayed in Fig. 7c). Therefore, the increasing Cu ion release between 60 and 120 min in case of *S. aureus* inoculated BTS visible in Fig. 4c may potentially be linked to an increase in Cu uptake by the exposure of the cytoplasm, accompanying cell wall disruption and cell death after extended contact to the Cu surfaces, which was previously averted by a more rigid cell wall of the gram-positive bacteria.

Based on these considerations, the deviation in measured Cu ion release between gram-positive *S. aureus* and gram-negative *E. coli* appears to be mainly related to strain-specific differences in membrane integrity, which affects Cu scavenging and thus Cu surface corrosion. In fact, the thickened surface oxide layer formation as well as the reduced

Cu ion release of USP-DLIP Cu surfaces under exposure to *S. aureus* befits previous observations of increased surface passivation in PBS by defect implantation alongside USP-DLIP in a recent study [49]. This shows a considerably lower Cu scavenging effect of *S. aureus*, which results in lower Cu ion release rates on USP-DLIP compared to smooth surfaces. However, this does not appear to limit an enhancement of bactericidal activity by contact promoting topographies.

3. Conclusions

The impact of topographically modified contact conditions on antibacterial efficacy of Cu surfaces has been investigated for gram-negative *E. coli* and gram-positive *S. aureus*. The conclusions of the study can be summarized as follows:

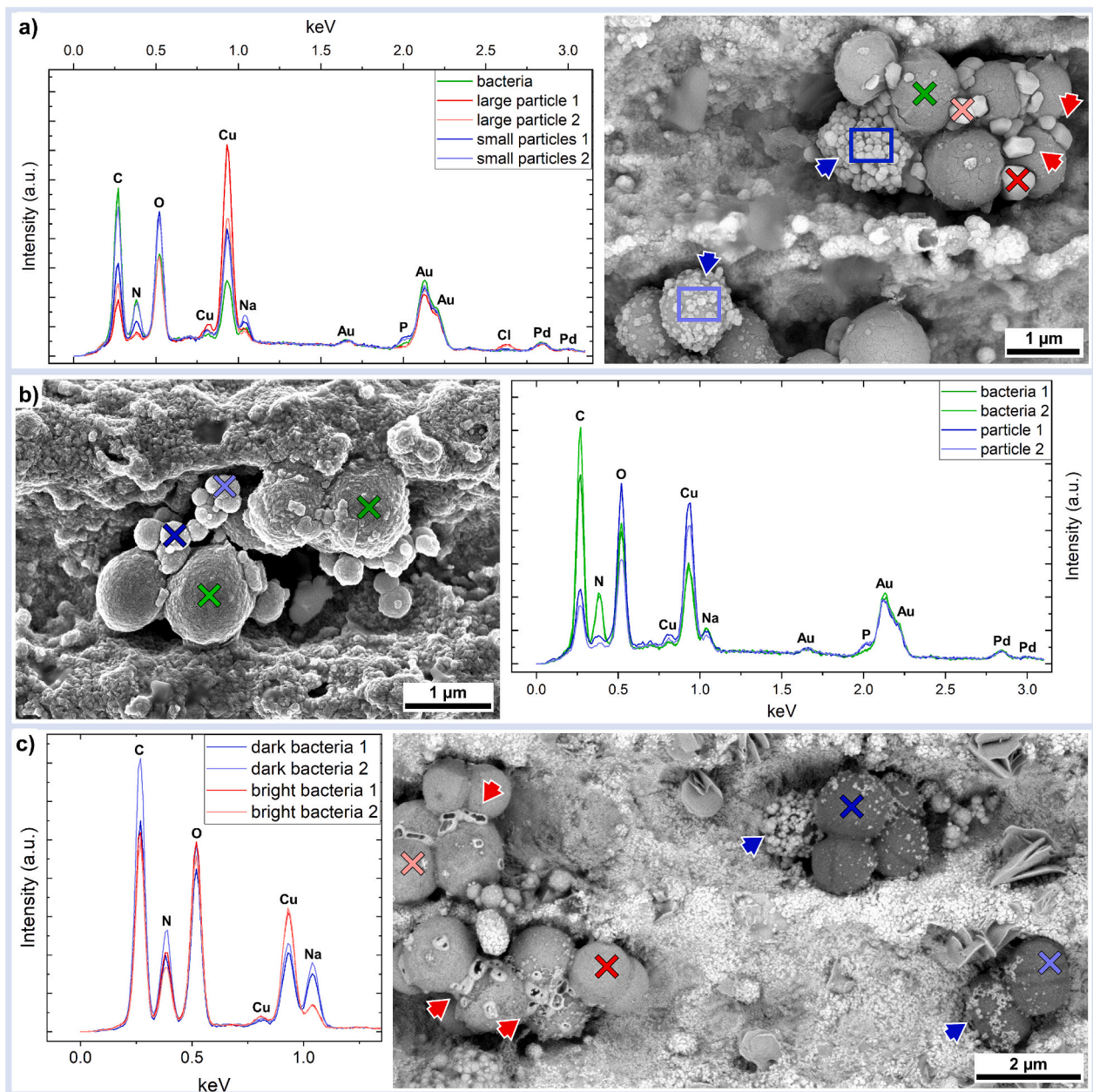


Fig. 7. EDS analysis of a) different particles found attached to *S. aureus* bacterial cells on coated samples imaged in BSE-contrast at 10 kV, b) spherical particle clusters in the periphery of bacterial cells imaged in SE-contrast, c) uncoated bacteria exhibiting different Z-contrast in BSE-imaging at 1.5 keV acceleration voltage. Large and small particle types are exemplarily marked by red and blue arrows in a) and c). (For interpretation of the references to colour in this figure legend, the reader is referred to the web version of this article.)

- Increased Bacteria/Substrate Contact and Antibacterial efficacy:** Topographic surface modification by USP-DLIP that allows for a larger contact area between bacteria and the substrate is associated with increased bactericidal activity. Bacterial killing rates on these surfaces might level several orders of magnitude higher than the smooth reference surfaces. The USP-DLIP topography that exhibit the highest bactericidal efficacy varies between the two tested strains. In the case of *S. aureus*, the bacteria-specific tendency to cluster formation appears to reduce the capability of individual bacterial cells to achieve high surface contact within the topographic trenches close to single bacterial scale. Instead, an increased cavity scale that allows intrusion of whole cell clusters was shown to be highly effective in increasing bactericidal efficacy against *S. aureus*. This results in higher pattern scales that are associated with increased bactericidal activity despite lower statistical cell diameters

compared to *E. coli*, which is most efficiently killed on surfaces allowing high single cell contact. Pattern scales below the single bacterial cell size tend to decrease both antibacterial efficacy and Cu sensitivity for both strains.

- Antimicrobial Efficacy and Cu Ion Release:** Antimicrobial efficacy of Cu surfaces against *E. coli* and *S. aureus* is found to be less dependent on the quantity of Cu ion release, but rather scales with the extend of contact area between individual adherent cells and substrate. Surface topographies that provide high single cell contacts appear to trigger an increased sensitivity for environmental Cu, where bactericidal activity is enhanced independent from quantitative Cu emission. Based on this, contact dependent Cu sensitivity appears to be the main driving force behind deviating antimicrobial activity between the different tested surface topographies.

- **Strain specific Cu Interaction:** Wet plating in PBS was found to involve Cu scavenging mechanisms in both bacterial strains that catalyzes Cu ion release over natural passivation. This effect is more pronounced in *E. coli*, where the bacterial cells seem to be less protected against involuntary Cu uptake due to the weaker cell membrane, while Cu accumulation may be additionally driven by chemical microcell formation. In the case of *S. aureus*, Cu scavenging is reduced, which additionally results in higher surface passivation of USP-DLIP processed samples. Initial Cu accumulation in *S. aureus* involves the agglomeration of extracellular Cu phosphate particles via membrane nucleation. Increased membrane stress finally appears to induce a step-wise collapse of the cell wall followed by an exposure of cytoplasm and a quantitative increase in Cu uptake under further extended Cu exposure.

The results of this study demonstrate that targeted surface design by USP-DLIP, involving topographic and chemical surface modification, can potentially increase antimicrobial surface efficiency with less dependency on quantitative Cu ion release. In parallel, peculiarities of strain specific surface interactions are showcased that need to be considered to enable targeted surface tailoring. This provides a valuable foundation to further investigate and potentially incorporate bacterial interactions into advanced decontamination concepts including strain-specific adaptation strategies for critical environments [6,7,31].

4. Methods

4.1. Sample preparation

For further surface modification and testing, single samples of the dimensions $10 \times 25 \text{ mm}^2$ have been charted from 1 mm sheets of oxygen free Cu (>99.95 %) (*Wieland*) and AISI 304 stainless steel (*Brio*) In case of stainless steel, the material was purchased in mirror-polished condition ($R_a < 10 \text{ nm}$), while Cu samples underwent polishing on an automated *TegraPol-21* system (*Struers*) to reach equivalent initial surface roughness [59]. Shares of the polished samples are deducted to provide reference surfaces of flat topography (denoted as Steel Ref. and Cu Ref.).

Mirror-polished samples of Cu are subjected to USP-DLIP inducing line-like periodic surface patterns in the scale of either $3 \mu\text{m}$ ($P > Bac$), $1 \mu\text{m}$ ($P \approx Bac$) or 750 nm ($P < Bac$). In the USP-DLIP setup a Ti:Sapphire *Spitfire* laser system (*Spectra Physics*) is utilized, operating at $t_p = 100 \text{ fs}$ pulse duration (FWHM), 1 kHz repetition rate and a centered wavelength λ of 800 nm . Line-like surface patterns are generated by two beam laser interference using a previously introduced optical setup [60] consisting of a diffractive optical element (DOE) to split and a lens system to recombine the partial beams on the substrate surface. To create the different pattern periodicities P the optical setup has been modified to adjust the single beam incident angle θ according to Eq. (1):

$$P = \frac{\lambda}{2 \sin(\theta)} \quad (1)$$

With $P = 3 \mu\text{m} \rightarrow \theta = 7.66^\circ$, $P = 1 \mu\text{m} \rightarrow \theta = 23.58^\circ$ and $P = 750 \text{ nm} \rightarrow \theta = 32.23^\circ$. Planar patterning was conducted by scanning the substrate surface in continuous pulsing mode adjusting the fluence and pulse overlap according to the individual material ablation threshold and pattern scale specific impact of ablation kinetics in pattern formation using p-polarized two-beam USP-DLIP [44]: $3 \mu\text{m}$ patterns have been produced with an overlapping pulse count of $N = 10$ at 2.14 J/cm^2 , while for $1 \mu\text{m}$ and 750 nm patterns reduced pulse counts of $N = 3$ and 2 at fluences of 1.38 J/cm^2 were applied. One batch of Cu samples subsequently underwent ultrasonic assisted immersion etching in 3 % citric acid for 40 s to remove process-induced oxidic substructures [45]. The other batch of the Cu samples remained unaffected (as-processed samples).

4.2. Surface characterization

Surface characterization of the different samples with and without USP-DLIP treatment was conducted by means of both confocal laser scanning microscopy (CLSM) (*LEXT OLS4100* by *Olympus*) and scanning electron microscopy (SEM) (*Helios Nanolab 600* by *FEI* and *Helios PFIB G4 CXe* by *Thermo Fisher*) also including the system's focused ion beam (FIB) and energy-dispersive X-ray spectroscopy (EDS) modules.

The CLSM analysis involved a $50\times$ objective (NA 0.95) with altered digital magnification of either $2\times$ or $6\times$ at a laser wavelength of 405 nm . The surface geometry of the various topographies applied using USP-DLIP was quantified based on periodicity, valley/peak ratio, valley width and depth, and surface ratio, defined as the ratio between the actual surface and an idealized smooth reference surface. Each parameter was measured on six individual spots on three different samples per topography for statistical evaluation comprising the determination of both the arithmetic mean value (MV) and standard deviation.

High resolution SEM imaging was conducted in secondary electron (SE) contrast mode at an acceleration voltage of 5 kV and a current of 86 pA at 52° sample tilt for improved visualization of topographic morphology. High resolution imaging was conducted using the in-lens detector in immersion mode. Furthermore, low voltage backscatter electron (BSE) images of uncoated samples were acquired using a solid state detector at 0° sample tilt. To assess the initial state of surface oxide composition high resolution grazing incidence X-ray diffraction (GI-XRD, *PANalytical X'Pert PRO-MPD*) was applied utilizing $\text{Cu K}\alpha$ radiation with a Goebel mirror at a 1° grazing angle in parallel orientation to the line-like patterns to avoid shadowing of the valley surface compartments. Within this setup 95 % of the measured signal can be estimated to originate from an interaction volume within a depth of $<1.11 \mu\text{m}$ from the substrate surface [61].

After surface exposure during wet plating, the bacteria/substrate contact as well as the induced damage on both bacterial cells and Cu substrate were investigated by SEM imaging, FIB cross-sectioning, and EDS analysis at an acceleration voltage of 1.5 kV to 10 kV (BSE-SEM), 30 kV (Ga-ion beam) and 5 kV (EDS), respectively. The low acceleration voltage chosen for EDS was shown to enable a more surface sensitive spectroscopic assessment of element composition, in a previous study [45]. For FIB cross-sectioning, an additional contrast layer of $\sim 10 \text{ nm}$ $\text{Au}_{80}\text{Pd}_{20}$ was applied by sputter coating before covering the investigated site with a protective layer of electron and ion beam induced Pt-deposition to preserve the substrate surface from ion-induced degradation. For EDS measurements, the sample was rotated to align the line pattern on the surface with the azimuth angle of the detector to avoid shadowing. SE imaging to investigate bacterial contact condition has been conducted at ten different locations on samples of immersion etched USP-DLIP Cu surfaces and both the Cu and stainless steel references, whereas in-depth investigation of chemical surface modification for *S. aureus* was executed on representative locations chosen from this.

4.3. Surface wettability

Contact angle (CA) measurements were conducted to monitor the parallel influx of wettability on bacteria/surface interaction aside of surface topography. The samples have been tested after three weeks of aging in ambient condition, where surface wettability alteration after USP-DLIP processing can be considered as stabilized [43]. The static contact angle was monitored in triplicates for each surface by means of a Drop Shape Analysator *DSA 100* (*Krüss GmbH*) using distilled water at a fixed droplet volume of $3 \mu\text{l}$. Statistical evaluation involved the determination of the arithmetic MV and standard deviation for the CA measured on the different surfaces. The CA was detected both in orthogonal and parallel orientation to also include anisotropic droplet propagation on the line-like surface patterns.

4.4. Wet plating

E. coli K12 (BW25113) was cultured via aerobically overnight growth in lysogeny broth (LB) medium for 12 h at 37 °C with a shaking speed of 220 rpm according to Molteni et al. [62]. Bacterial cells in the stationary growth phase were collected from 5 ml culture medium by centrifugation for 15 min at 5000 ×g, which is followed by three consecutive PBS washing steps involving identical centrifugation parameters. Finally, the bacteria testing solution (BTS) was gained by resuspension in 5 ml of PBS. The hence achieved initial average cell count ranges in the scale of 9 log CFU/ml. Prior to cultivation, the *E. coli* bacteria have been stored for two weeks at 4 °C on agar plates after cultivation from cryo-storage at –81 °C, which have been provided by the Helmholtz Institute for Pharmaceutical Research Saarland (HIPS).

For the preparation of BTS containing *S. aureus* a single bacterial colony from a previously prepared blood agar plate was added to 5 ml tryptic soy broth (TSB). The bacterial solution was cultivated for 16 h at 37 °C and 150 rpm in an incubator. Afterwards, 40 µl of the bacterial solution was transferred into 4 ml of TSB. To obtain bacteria in the exponential phase this suspension was placed for 2.5 h at 37 °C and 150 rpm in the incubator. Subsequently, washing and centrifugation was performed, where 1 ml of the bacterial suspension was centrifuged for 3 min at 17000 g, followed by three washing steps in PBS. Before cultivation, the *S. aureus* bacteria have been stored on blood agar plates at 4 °C for less than two weeks after cultivation from a cryo-storage in glycerol stock at –20 °C. The utilized *S. aureus* wild-type strain SA113 (ATCC 35556) was provided by the Institute of Medical Microbiology and Hygiene of the Saarland University medical center.

Following the wet plating method for heterogeneous surface wetting properties described in a previous work [43], three droplets of 40 µl of the BTS were applied to individual exposure areas predefined by polyvinyl chloride (PVC) rings exhibiting an inner circular diameter of 5 mm. The slightly hydrophobic PVC prevent BTS spreading in case of hydrophilic and provide anchoring edges to facilitate complete droplet covering of the exposure area in case of (super-)hydrophobic surfaces. Each sample was stored in water saturated environment at ambient temperature during BTS exposure. Two doses of 5 µl each were withdrawn after three individual exposure intervals, each time probing a different droplet. Bacterial survival on the Cu surfaces was initially monitored to define suitable exposure durations that allow for a comparative assessment of bacterial viability on the different surfaces, where complete killing of both bacterial strains could be initially ascertained after 120 min of exposure. Due to the varying resilience of the tested bacterial strains, *E. coli* cells were exposed for 20 min, 40 min and 60 min, while *S. aureus* survival was monitored for 30 min, 60 min and 120 min. Bacteria adhering to the surface were resuspended by vigorous pipetting with a parallel tip orientation to the surface pattern to avoid shadowing of the pattern valleys. The number of viable bacteria was assessed using the standard plate count method by serial dilution of one of the 5 µl doses in PBS followed by plating on LB/blood agar plates. The inoculated agar plates were incubated overnight at 37 °C and 80 % moisture followed by counting of the remaining colony forming units (CFU) after the individual exposure intervals. The second 5 µl was diluted 600-fold dilution in 0.1 % HNO₃ for further determination of the corresponding Cu ion concentrations in the BTS by inductively coupled plasma triple quadrupole mass spectrometry (ICP-QQQ, Agilent 8900 ICP-QQQ). The experiments were conducted in triplicates on separate dates for each bacterial strain, where the evaluation of the statistical variation of both CFU decrease and Cu-ion release is determined via arithmetic MV and standard deviation.

In order to exclude the effect of surface enlargement by USP-DLIP on bacterial viability as well as quantitative Cu ion release, the CFU and ICP-QQQ results determined were normalized to a standardized surface area and exposure duration, thus allowing for a more accurate comparison. The corresponding CFU reduction and Cu ion release rate were defined by Eqs. (2) and (3).

$$\text{CFU reduction rate} = \frac{\text{CFU}}{t_{\text{exp}} A S} \ln \left(\frac{\text{CFU}}{\text{mincm}^2} \right) \quad (2)$$

$$\text{Cu ion release rate} = \frac{\text{Cu}_{\text{emitted}}}{t_{\text{exp}} A S} \ln \left(\frac{\mu\text{M}}{\text{mincm}^2} \right) \quad (3)$$

Here, CFU accounts to the viable colony forming units per ml and Cu_{emitted} to the release of Cu in µM detected after a defined exposure interval *t*_{exp}. A is the exposed surface area of 0.196 cm² defined by the circular PVC rings and S corresponds to the individual surface ratio denoted in Fig. 1, where S = 1 in the case of the smooth reference surfaces.

To allow for a better interpretation of the impact of the individual USP-DLIP surface modifications on both CFU reduction and Cu ion release rate, the deviation between the values measured on the different USP-DLIP surface types and the Cu references was calculated by Eq. (4) utilizing the arithmetic MV and supplemented in the bar graphs in Figs. 3 and 4.

$$\Delta_{\text{CFU reduction rate}} | \Delta_{\text{Cu ion release rate}} = \frac{MV_{\text{USP-DLIP}}}{MV_{\text{Cu Ref.}}} \quad (4)$$

The resulting factor Δ indicates an increase (> 1) or decrease (< 1) of both the CFU reduction and Cu ion release rate by the respective USP-DLIP treatment in comparison to the Cu references.

CRediT authorship contribution statement

Daniel Wyn Müller: Writing – review & editing, Writing – original draft, Visualization, Validation, Project administration, Methodology, Investigation, Funding acquisition, Formal analysis, Data curation, Conceptualization. **Christoph Pauly:** Writing – review & editing, Validation, Methodology, Investigation, Formal analysis. **Kristina Brix:** Writing – review & editing, Validation, Methodology, Investigation, Formal analysis, Data curation. **Ralf Kautenburger:** Writing – review & editing, Validation, Supervision, Resources, Methodology, Formal analysis, Data curation. **Frank Mücklich:** Writing – review & editing, Validation, Supervision, Resources, Project administration, Funding acquisition.

Author contributions

D.W. Müller conceived the idea, designed the interference-based laser setup used in this study and conducted sample preparation, surface characterization via confocal laser scanning microscopy (LSM), CA measurement, GI-XRD-analysis, scanning electron microscopy (SEM) for bacterial imaging and the wet plating experiments with additional support in the S2 level experiments involving the *S. aureus* strain. Post-mortem SEM-analysis of *S. aureus* cells including FIB cross-sectioning, STEM and EDS was carried out by D.W. Müller and C. Pauly. K. Brix and R. Kautenburger performed the inductively-coupled-plasma mass spectrometry (ICP-QQQ) analysis. Data interpretation and preparation of the manuscript was done by D.W. Müller and C. Pauly. F. Mücklich supervised the work.

Declaration of competing interest

The authors declare the following financial interests/personal relationships which may be considered as potential competing interests: The corresponding Author Daniel Wyn Müller is currently employed at SurFunction GmbH. This employment started after finishing the work reported in this manuscript, which relates to his previous research activities at the University of Saarland and has therefore not been influenced by this employment. The company is not financially interested into this topic and did not contribute in any way to this work. The other authors declare that they have no known competing financial interests

or personal relationships that could have appeared to influence the work reported in this paper.

Acknowledgements

We would like to acknowledge the support of Hannah Heintz from the group of Prof. Karin Jacobs (Department of Experimental Physics, Saarland University) in the wet plating experiments including *S. aureus* as well as Dr. Flavio Soldera in SEM analysis and further discussion. This work has been funded by the German Research Foundation (DFG) within the project “Controlled bacterial interaction to increase the antimicrobial efficiency of copper surfaces” (project number 415956642) and the German Aerospace Center – German Space Agency (DLR) within the project “Investigation of antimicrobial metal surfaces under space conditions - An effective strategy to prevent microbial biofilm formation”(project number 50WB1930). The authors acknowledge financial support in the project “MatInnovat” supported by the Saarland State Ministry of Economics with resources from the European Regional Development Fund (ERDF) and funding by the German Research Foundation for the PFIB/SEM system (*Helios PFIB G4 CXe* by *Thermo Fisher*) used in SEM analysis (DFG, INST 256/510-1 FUGG) and for the ICP-QQQ instrument used for elemental quantification (DFG, INST 256/553-1 FUGG).

Appendix A. Supplementary data

Supplementary data to this article can be found online at <https://doi.org/10.1016/j.bioadv.2025.214184>.

Data availability

Data will be made available on request.

References

- M. Naghavi, Global mortality associated with 33 bacterial pathogens in 2019: a systematic analysis for the global burden of Disease study 2019, *Lancet* 6736 (2022) 02185, [https://doi.org/10.1016/S0140-6736\(22\)02185-7](https://doi.org/10.1016/S0140-6736(22)02185-7).
- M. Cámara, W. Green, C.E. MacPhee, P.D. Rakowska, R. Raval, M.C. Richardson, J. Slater-Jefferies, K. Steventon, J.S. Webb, Economic significance of biofilms: a multidisciplinary and cross-sectoral challenge, *Npj Biofilms and Microbiomes* 8 (2022) 1–8, <https://doi.org/10.1038/s41522-022-00306-y>.
- C.J. Murray, K.S. Ikuta, F. Sharara, L. Swetschinski, G. Robles Aguilar, A. Gray, et al., Global burden of bacterial antimicrobial resistance in 2019: A systematic analysis, *Lancet* 399 (2022) 629–655, [https://doi.org/10.1016/S0140-6736\(21\)02724-0](https://doi.org/10.1016/S0140-6736(21)02724-0).
- L.-Y. Sobisch, K.M. Rogowski, J. Fuchs, W. Schmieder, A. Vaishampayan, P. Oles, N. Novikova, E. Grohmann, Biofilm forming antibiotic resistant gram-positive pathogens isolated from surfaces on the international Space Station, *Front. Microbiol.* 10 (2019) 1–16, <https://doi.org/10.3389/fmicb.2019.00543>.
- C. Urbaniak, M.D. Morrison, J.B. Thissen, F. Karouia, D.J. Smith, S. Mehta, C. Jaing, K. Venkateswaran, Microbial Tracking-2, a metagenomics analysis of bacteria and fungi onboard the international Space Station, *Microbiome* 10 (2022) 1–19, <https://doi.org/10.1186/s40168-022-01293-0>.
- E.A. Bryce, B. Velapattino, H. Akbari Khorami, T. Donnelly-Pierce, T. Wong, R. Dixon, E. Asselin, In vitro evaluation of antimicrobial efficacy and durability of three copper surfaces used in healthcare, *Biointerphases* 15 (2020) 011005, <https://doi.org/10.1116/1.5134676>.
- M. Colin, E. Charpentier, F. Klingelschmitt, C. Bontemps, C. De Champs, F. Reffuveille, S.C. Gangloff, Specific antibacterial activity of copper alloy touch surfaces in five long-term care facilities for older adults, *J. Hosp. Infect.* 104 (2020) 283–292, <https://doi.org/10.1016/j.jhin.2019.11.021>.
- A. Tripathy, P. Sen, B. Su, W.H. Briscoe, Natural and bioinspired nanostructured bactericidal surfaces, *Adv. Colloid Interf. Sci.* 248 (2017) 85–104, <https://doi.org/10.1016/j.cis.2017.07.030>.
- L. Pellegrino, L.S. Kriem, E.S.J. Robles, J.T. Cabral, Microbial response to micrometer-scale multiaxial wrinkled surfaces, *ACS Appl. Mater. Interfaces* 14 (2022) 31463–31473, <https://doi.org/10.1021/acsmi.2c08768>.
- M. Hans, J.C. Támara, S. Mathews, B. Bax, A. Hegetschweiler, R. Kautenburger, M. Solioz, F. Mücklich, Laser cladding of stainless steel with a copper-silver alloy to generate surfaces of high antimicrobial activity, *Appl. Surf. Sci.* 320 (2014) 195–199, <https://doi.org/10.1016/j.apsusc.2014.09.069>.
- T.L. Meister, J. Fortmann, M. Breisch, C. Sengstock, E. Steinmann, M. Köller, S. Pfaender, A. Ludwig, Nanoscale copper and silver thin film systems display differences in antiviral and antibacterial properties, *Sci. Rep.* 12 (2022) 1–10, <https://doi.org/10.1038/s41598-022-11212-w>.
- H.T. Michels, J.O. Noyce, C.W. Keevil, Effects of temperature and humidity on the efficacy of methicillin-resistant *Staphylococcus aureus* challenged antimicrobial materials containing silver and copper, *Lett. Appl. Microbiol.* 49 (2009) 191–195, <https://doi.org/10.1111/j.1472-765X.2009.02637.x>.
- S. Krupanidhi, A. Sreekumar, C.B. Sanjeevi, Copper & biological health, 2008, <https://doi.org/10.1080/10937400600755911>.
- S. Kim, J.E. Choi, J. Choi, K.H. Chung, K. Park, J. Yi, D.Y. Ryu, Oxidative stress-dependent toxicity of silver nanoparticles in human hepatoma cells, *Toxicol. in Vitro* 23 (2009) 1076–1084, <https://doi.org/10.1016/j.tiv.2009.06.001>.
- M. Hans, S. Mathews, F. Mücklich, M. Solioz, Physicochemical properties of copper important for its antibacterial activity and development of a unified model, *Biointerphases* 11 (2016) 018902, <https://doi.org/10.1116/1.4935853>.
- M. Solioz, Copper disposition in bacteria, in: *Clinical and Translational Perspectives on WILSON DISEASE*, 2019, pp. 101–113, <https://doi.org/10.1016/B978-0-12-810532-0.00011-2>.
- S. Mathews, M. Hans, F. Mücklich, M. Solioz, Contact killing of bacteria on copper is suppressed if bacterial-metal contact is prevented and is induced on iron by copper ions, *Appl. Environ. Microbiol.* 79 (2013) 2605–2611, <https://doi.org/10.1128/AEM.03608-12>.
- M. Hans, A. Erbe, S. Mathews, Y. Chen, M. Solioz, F. Mücklich, Role of copper oxides in contact killing of bacteria, *Langmuir* 29 (2013) 16160–16166, <https://doi.org/10.1021/la404091z>.
- E. Fadeeva, V.K. Truong, M. Stiesch, B.N. Chichkov, R.J. Crawford, J. Wang, E. P. Ivanova, Bacterial retention on superhydrophobic titanium surfaces fabricated by femtosecond laser ablation, *Langmuir* 27 (2011) 3012–3019, <https://doi.org/10.1021/la104607g>.
- A. Elbourne, R.J. Crawford, E.P. Ivanova, Nano-structured antimicrobial surfaces: from nature to synthetic analogues, *J. Colloid Interface Sci.* 508 (2017) 603–616, <https://doi.org/10.1016/j.jcis.2017.07.021>.
- N. Epperlein, F. Menzel, K. Schwibbert, R. Koter, J. Bonse, J. Sameith, J. Krüger, J. Toepel, Influence of femtosecond laser produced nanostructures on biofilm growth on steel, *Appl. Surf. Sci.* 418 (2017) 420–424, <https://doi.org/10.1016/j.apsusc.2017.02.174>.
- D. Guenther, J. Valle, S. Burgui, C. Gil, C. Solano, D. Guenther, J. Valle, S. Burgui, C. Gil, C. Solano, A. Toledo-arana, R. Helbig, C. Werner, I. Lasa, F. Andrés, Direct Laser Interference Patterning for Decreased Bacterial Attachment, in: *SPIE 9736, Laser-Based Micro- and Nanoprocessing X*, 2016, <https://doi.org/10.1117/12.2216065>.
- R. Helbig, D. Günther, J. Friedrichs, F. Rößler, A. Lasagni, C. Werner, The impact of structure dimensions on initial bacterial adhesion, *Biomater. Sci.* 4 (2016) 1074–1078, <https://doi.org/10.1039/C6BM00078A>.
- J. Valle, S. Burgui, D. Langheinrich, C. Gil, C. Solano, A. Toledo-Arana, R. Helbig, A. Lasagni, I. Lasa, Evaluation of surface microtopography engineered by direct laser interference for bacterial anti-biofouling, *Macromol. Biosci.* 15 (2015) 1060–1069, <https://doi.org/10.1002/mabi.201500107>.
- L.C. Hsu, J. Fang, D.A. Borca-Tasciuc, R.W. Worobo, C.I. Moraru, Effect of micro- and nanoscale topography on the adhesion of bacterial cells to solid surfaces, *Appl. Environ. Microbiol.* 79 (2013) 2703–2712, <https://doi.org/10.1128/AEM.03436-12>.
- A.H.A. Lutey, L. Gemini, L. Romoli, G. Lazzini, F. Fuso, M. Faucon, R. Kling, Towards laser-textured antibacterial surfaces, *Sci. Rep.* 8 (2018) 1–10, <https://doi.org/10.1038/s41598-018-28454-2>.
- C. Berne, C.K. Ellison, A. Ducret, Y.V. Brun, Bacterial adhesion at the single-cell level, *Nat. Rev. Microbiol.* 16 (2018) 616–627, <https://doi.org/10.1038/s41579-018-0057-5>.
- T. Kimkes, M. Heinemann, How Bacteria recognise and respond to surface contact, *FEMS Microbiol. Rev.* 44 (2020) 106–122.
- E. Maikranz, C. Spengler, N. Thewes, A. Thewes, F. Nolle, P. Jung, M. Bischoff, L. Santen, K. Jacobs, Different binding mechanisms of *Staphylococcus aureus* to hydrophobic and hydrophilic surfaces, *Nanoscale* 12 (2020) 19267–19275, <https://doi.org/10.1039/d0nr03134h>.
- L.B. Boinovich, E.B. Modin, A.V. Aleshkin, K.A. Emelyanenko, E.R. Zulkarneev, I. A. Kiseleva, A.L. Vasiliev, A.M. Emelyanenko, Effective antibacterial Nanotextured surfaces based on extreme wettability and bacteriophage seeding, *ACS Appl. Nano Mater.* 1 (2018) 1348–1359, <https://doi.org/10.1021/acsnm.8b00090>.
- K. Siems, D.W. Müller, L. Maertens, A. Ahmed, R. Van Houdt, R.L. Mancinelli, S. Baur, K. Brix, R. Kautenburger, N. Caplin, J. Krause, R. Demets, M. Vukich, A. Tortora, C. Roesch, G. Holland, M. Laue, F. Mücklich, R. Moeller, Testing laser-structured antimicrobial surfaces under space conditions: the design of the ISS experiment BIOFILMS, *Front. Space Technol.* 2 (2022) 1–18, <https://doi.org/10.3389/frspt.2021.773244>.
- P. Flores, R. Schauer, S.A. McBride, J. Luo, M. Cortesão, C. Hoehn, S. Doraisingam, D. Widhalm, J. Chadha, H. Meyerson, E. Mitzak, V. Hurd, L. Selman, M. Vellone, S. Floyd, S. Tozer, M. Rupert, S. Gorti, S. Reagan, K.K. Varanasi, F. Muecklich, R. Moeller, L. Stodieck, S. Countryman, L. Zea, Preparation for and performance of a *Pseudomonas aeruginosa* biofilm experiment on board the international Space Station, *Acta Astronaut.* (2021), <https://doi.org/10.1016/j.actaastro.2022.07.015>.
- C. Chen, A. Enrico, T. Pettersson, M. Ek, A. Herland, F. Niklaus, G. Stemme, L. Wågberg, Bactericidal surfaces prepared by femtosecond laser patterning and layer-by-layer polyelectrolyte coating, *J. Colloid Interface Sci.* 575 (2020) 286–297, <https://doi.org/10.1016/j.jcis.2020.04.107>.
- A. Tripathy, S. Sreedharan, C. Bhaskarla, S. Majumdar, S.K. Peneti, D. Nandi, P. Sen, Enhancing the bactericidal efficacy of nanostructured multifunctional

- surface using an ultrathin metal coating, *Langmuir* 33 (2017) 12569–12579, <https://doi.org/10.1021/acs.langmuir.7b02291>.
- [35] V. Gopinath, S. Priyadarshini, A.R. Al-Maleki, M. Alagiri, R. Yahya, S. Saravanan, J. Vadivelu, In vitro toxicity, apoptosis and antimicrobial effects of phyto-mediated copper oxide nanoparticles, *RSC Adv.* 6 (2016) 110986–110995, <https://doi.org/10.1039/c6ra13871c>.
- [36] A.L. Ulloa-Ogaz, H.A. Piñón-Castillo, L.N. Muñoz-Castellanos, M.S. Athie-García, M.D.L. Ballinas-Casarrubias, J.G. Murillo-Ramírez, L.Á. Flores-Ongay, R. Duran, E. Orrantia-Borunda, Oxidative damage to *Pseudomonas aeruginosa* ATCC 27833 and *Staphylococcus aureus* ATCC 24213 induced by CuO-NPs, *Environ. Sci. Pollut. Res.* 24 (2017) 22048–22060, <https://doi.org/10.1007/s11356-017-9718-6>.
- [37] C.A.P. Bastos, N. Faria, J. Wills, P. Malmberg, N. Scheers, P. Rees, J.J. Powell, Copper nanoparticles have negligible direct antibacterial impact, *NanoImpact* 17 (2020) 100192, <https://doi.org/10.1016/j.impact.2019.100192>.
- [38] A.M. Emelyanenko, V.V. Kaminskii, I.S. Pytskii, A.G. Domantovsky, K. A. Emelyanenko, A.V. Aleshkin, L.B. Boinovich, Antibacterial properties of Superhydrophilic textured copper in contact with bacterial suspensions, *Bull. Exp. Biol. Med.* 168 (2020) 488–491, <https://doi.org/10.1007/s10517-020-04737-5>.
- [39] G. Yi, S.N. Riduan, A. Armugam, J.T. Ong, P.Y. Hon, M.Y. Abdad, S. Vasoo, B.S. P. Ang, Y. Zhang, Nanostructured copper surface kills ESKAPE pathogens and viruses in minutes, *ChemMedChem* 16 (2021) 3553–3558, <https://doi.org/10.1002/cmdc.202100504>.
- [40] A.M. Emelyanenko, I.S. Pytskii, V.V. Kaminsky, E.V. Chulkova, A.G. Domantovsky, K.A. Emelyanenko, V.D. Sobolev, A.V. Aleshkin, L.B. Boinovich, Superhydrophobic copper in biological liquids: antibacterial activity and microbiologically induced or inhibited corrosion, *Colloids Surf. B: Biointerfaces* 185 (2020) 110622, <https://doi.org/10.1016/j.colsurfb.2019.110622>.
- [41] L.B. Boinovich, K.A. Emelyanenko, A.G. Domantovsky, E.V. Chulkova, A. A. Shiryayev, A.M. Emelyanenko, Pulsed laser induced triple layer copper oxide structure for durable Polyfunctionality of Superhydrophobic coatings, *Adv. Mater. Interfaces* 5 (2018) 1–10, <https://doi.org/10.1002/admi.201801099>.
- [42] J.L. Smith, N. Tran, T. Song, D. Liang, M. Qian, Robust bulk micro-nano hierarchical copper structures possessing exceptional bactericidal efficacy, *Biomaterials* 280 (2022) 121271, <https://doi.org/10.1016/j.biomaterials.2021.121271>.
- [43] D.W. Müller, S. Lößlein, E. Terriac, K. Brix, R. Kautenburger, K. Siems, R. Möller, F. Mücklich, Increasing antibacterial efficiency of Cu surfaces by targeted surface functionalization via ultrashort pulsed direct laser interference patterning (USP-DLIP), *Adv. Mater. Interfaces* 8 (2021) 2001656, <https://doi.org/10.1002/admi.202001656>.
- [44] D.W. Müller, S. Lößlein, C. Pauly, M. Briesenick, G. Kickelbick, F. Mücklich, Multi-pulse agglomeration effects on ultrashort pulsed direct laser interference patterning of Cu, *Appl. Surf. Sci.* 611 (2023) 155538, <https://doi.org/10.1016/j.apsusc.2022.155538>.
- [45] D.W. Müller, A. Holtsch, S. Lößlein, C. Pauly, C. Spengler, S. Grandthyll, K. Jacobs, F. Mücklich, In-depth investigation of copper surface chemistry modification by ultrashort pulsed direct laser interference patterning, *Langmuir* 36 (2020) 13415–13425, <https://doi.org/10.1021/acs.langmuir.0c01625>.
- [46] L.B. Boinovich, V.V. Kaminsky, A.G. Domantovsky, K.A. Emelyanenko, A. V. Aleshkin, E.R. Zulkarneev, I.A. Kiseleva, A.M. Emelyanenko, Bactericidal activity of Superhydrophobic and Superhydrophilic copper in bacterial dispersions, *Langmuir* 35 (2019) 2832–2841, <https://doi.org/10.1021/acs.langmuir.8b03817>.
- [47] Y. Cheng, G. Feng, C.I. Moraru, Micro-and nanotopography sensitive bacterial attachment mechanisms: a review, *Front. Microbiol.* 10 (2019) 1–17, <https://doi.org/10.3389/fmicb.2019.00191>.
- [48] S. Marie Lößlein, R. Merz, Y. Rodríguez-Martínez, F. Schäfer, P.G. Grützmacher, D. Horwat, M. Kopnarski, F. Mücklich, Influence of chemistry and topography on the wettability of copper, *J. Colloid Interface Sci.* 670 (2024) 658–675, <https://doi.org/10.1016/j.jcis.2024.04.212>.
- [49] D.W. Müller, B. Josten, S. Wältermann, C. Pauly, S. Slawik, K. Brix, R. Kautenburger, F. Mücklich, Microstructure versus topography: the impact of crystallographic substrate modification during ultrashort pulsed direct laser interference patterning on the antibacterial properties of Cu, *Front. Mater.* 11 (2024) 1397937, <https://doi.org/10.3389/fmats.2024.1397937>.
- [50] C. Formosa-Dague, C. Feuillie, A. Beaussart, S. Derclaye, S. Kucharíková, I. Lasa, P. Van Dijk, Y.F. Dufreine, Sticky matrix: adhesion mechanism of the staphylococcal polysaccharide intercellular Adhesin, *ACS Nano* 10 (2016) 3443–3452, <https://doi.org/10.1021/acs.nano.5b07515>.
- [51] Y.F. Dufreine, A. Persat, Mechanomicrobiology: how bacteria sense and respond to forces, *Nat. Rev. Microbiol.* 18 (2020) 227–240, <https://doi.org/10.1038/s41579-019-0314-2>.
- [52] C. Spengler, E. Maikranz, B. Glatz, M.A. Klatt, H. Heintz, M. Bischoff, L. Santen, A. Fery, K. Jacobs, The adhesion capability of *Staphylococcus aureus* cells is heterogeneously distributed over the cell envelope, *Soft Matter* 20 (2024), <https://doi.org/10.1039/D3SM01045G>.
- [53] J. Luo, C. Hein, J. Ghanbaja, J. Pierson, F. Mücklich, Bacteria accumulate copper ions and inhibit oxide formation on copper surface during antibacterial efficiency test, *Micron* 127 (2019) 102759.
- [54] K. Alasvand Zarasvand, V.R. Rai, Microorganisms: induction and inhibition of corrosion in metals, *Int. Biodeterior. Biodegrad.* 87 (2014) 66–74, <https://doi.org/10.1016/j.ibiod.2013.10.023>.
- [55] G. He, W. Hu, C.M. Li, Spontaneous interfacial reaction between metallic copper and PBS to form cupric phosphate nanoflower and its enzyme hybrid with enhanced activity, *Colloids Surf. B: Biointerfaces* 135 (2015) 613–618, <https://doi.org/10.1016/j.colsurfb.2015.08.030>.
- [56] M.T. González-Muñoz, C. Rodríguez-Navarro, F. Martínez-Ruiz, J.M. Arias, M. L. Merroun, M. Rodríguez-Gallego, Bacterial biomineralization: new insights from *Myxococcus*-induced mineral precipitation, *Geol. Soc. Lond. Spec. Publ.* 336 (2010) 31–50, <https://doi.org/10.1144/SP336.3>.
- [57] N. Ben Omar, M.M. Nez-canamero, J.M. Arias, F. Huertas, *Myxococcus xanthus* killed cells as inducers of struvite crystallization, its possible role in the biomineralization processes, *Chemosphere* 30 (1995) 2387–2396.
- [58] P. Wang, T.B. Kinraide, E. Smolders, D.M. Zhou, N.W. Menzies, S. Thakali, W. W. Xia, X.Z. Hao, W.J.G.M. Peijnenburg, P.M. Kopittke, An electrostatic model predicting Cu and Ni toxicity to microbial processes in soils, *Soil Biol. Biochem.* 57 (2013) 720–730, <https://doi.org/10.1016/j.soilbio.2012.09.002>.
- [59] S.M. Lößlein, M. Kasper, R. Merz, C. Pauly, D.W. Müller, M. Kopnarski, F. Mücklich, Patience alone is not enough - a guide for the preparation of low-defect sections from pure copper Geduld allein reicht nicht! - Ein Leitfaden zur Herstellung defektarmer Schiffe von Reinkupfer, *Praktische Metallographie/practical, Metallography* 58 (2021) 388–407, <https://doi.org/10.1515/pm-2021-0031>.
- [60] D.W. Müller, T. Fox, P.G. Grützmacher, S. Suarez, F. Mücklich, Applying ultrashort pulsed direct laser interference patterning for functional surfaces, *Sci. Rep.* 10 (2020) 3647, <https://doi.org/10.1038/s41598-020-60592-4>.
- [61] B.D. Cullity, S.R. Stock, *Elements of X-Ray Diffraction*, 2001.
- [62] C. Molteni, H.K. Abicht, M. Solioz, Killing of Bacteria by copper surfaces involves dissolved copper, *Appl. Environ. Microbiol.* 76 (2010) 4099–4101, <https://doi.org/10.1128/AEM.00424-10>.